VU Research Portal

Flooding of the Caspian Sea at the intensification of Northern Hemisphere Glaciations

Van Baak, Christiaan G.C.; Grothe, Arjen; Richards, Keith; Stoica, Marius; Aliyeva, Elmira; Davies, Gareth R.; Kuiper, Klaudia F.; Krijgsman, Wout

document version
Publisher's PDF, also known as Version of record

document license
Article 25fa Dutch Copyright Act

Link to publication in VU Research Portal

Research article

Flooding of the Caspian Sea at the intensification of Northern Hemisphere Glaciations

Christiaan G.C. Van Baak[a,b,*], Arjen Grothe[a,c], Keith Richards[d,e], Marius Stoica[f], Elmira Aliyeva[g], Gareth R. Davies[h], Klaudia F. Kuiper[h], Wout Krijgsman[a]

[a] Paleomagnetic Laboratory "Fort Hoofddijk", Budapestlaan 17, 3584 CD Utrecht, The Netherlands
[b] CASP, West Building, Madingley Rise, Madingley Road, CB3 0UD Cambridge, United Kingdom
[c] Marine Palynology and Paleoceanography, Laboratory of Palaeobotany and Palynology, Utrecht University, Vening Meineszgebouw A, Princetonlaan 8a, 3584 CB Utrecht, The Netherlands
[d] KrA Stratigraphic Ltd., United Kingdom
[e] Institute for Biodiversity and Ecosystem Dynamics (IBED), University of Amsterdam, The Netherlands
[f] Department of Geology, Faculty of Geology and Geophysics, University of Bucharest, Bălcescu Bd.1, Bucharest 010041, Romania
[g] Geological Institute of Azerbaijan (GIA), H. Javid Av. 29A, AZ1143 Baku, Azerbaijan
[h] Faculty of Science, Vrije Universiteit (VU) Amsterdam, De Boelelaan 1085, 1081 HV Amsterdam, The Netherlands

ARTICLE INFO

ABSTRACT

The semi-isolated epicontinental Paratethys Sea in the Eurasian continental interior was highly sensitive to changes in basin connectivity and hydrological budget. The Caspian Sea, the easternmost basin experienced a five-fold increase in surface area during the Plio-Pleistocene climate transition, but a basic process-based understanding is severely hampered by a lack of high-resolution age constraints. Here, we present a magnetostratigraphic age model supported by $^{40}Ar/^{39}Ar$ dating of volcanic ash layers for the 1600 m thick Jeirankechmez section in Azerbaijan that comprises a sedimentary rock succession covering this so-called Akchagylian flooding. We establish the age of this major change in Caspian paleohydrology at around 2.7 Ma. The presence of cold water foraminifera, rising strontium isotope ratios and the possible arrival of the enigmatic Caspian seal in the basin hints at an Arctic marine source for the Akchagylian waters. The new age model indicates a direct link to the intensification of northern hemisphere glaciations at the end of the Pliocene and to concurrent hydrological shifts across Eurasia, such as the onset of cyclic Chinese Loess deposits. The transformation of the Paratethys region around 2.7 Ma from a series of small Pliocene endorheic lake basins to a large Early Pleistocene epicontinental water mass coincides with a more positive hydrological budget for the Eurasian continental interior. The drainage of additional high latitude, low salinity water to the Mediterranean, may have contributed towards variability in global paleoceanography, and could potentially provide a positive feedback towards Pleistocene climate cooling.

1. Introduction

Semi-isolated basins like the Mediterranean and Paratethys (former Black Sea-Caspian Sea domain) are exceptionally suited for the study of (paleo-) environmental changes as a function of relative sea level fluctuations. These land-locked areas are at present only connected to the open ocean via shallow and narrow gateways, and decreased hydrological exchange had profound influences on environmental conditions (e.g. temperature, salinity, humidity; de la Vara et al., 2016). For example, increased Mediterranean-Paratethys connectivity played an important role during the latest Messinian (Van Baak et al., 2016,

2017), drastically changing salinities in both basins (Krijgsman et al., 2010; van Baak et al., 2015), allowing bidirectional faunal exchange (Stoica et al., 2013; Grothe et al., 2018). Sea level dropped in the basins and both Paratethys and Mediterranean temporarily transformed into enormous endorheic lakes.

Paratethys water level changes can indirectly influence the hydrological budget of the Mediterranean Sea and at the same time control temperatures on the Eurasian continent. A large Paratethys sea acts as a thermal regulator, allowing an oceanic climate to develop over the continental interior of Eurasia, thereby decreasing Eurasian summer temperatures and as a result decreasing the strength of the South Asian
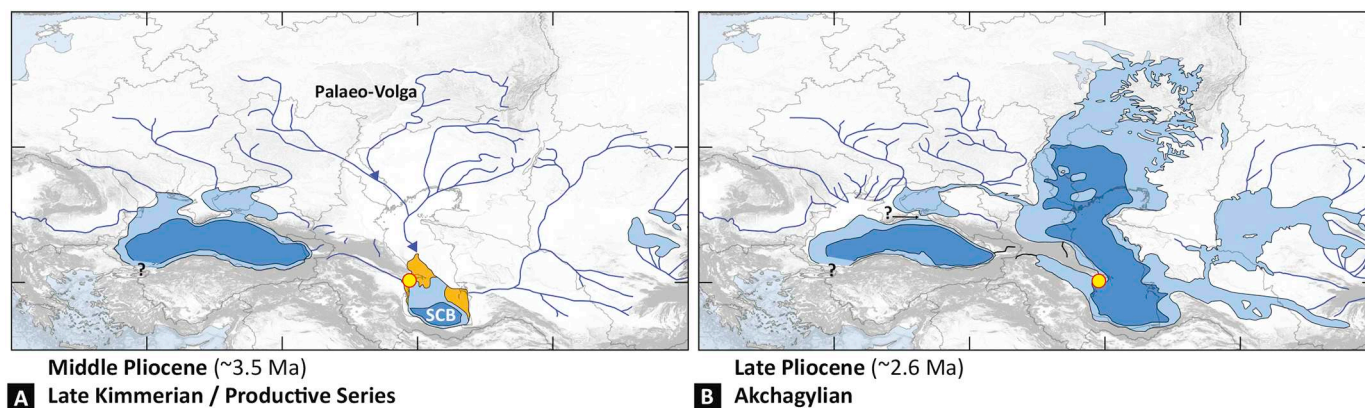
Fig. 1. Paleogeographic reconstructions of the a) Middle Pliocene and b) Latest Pliocene, Early Pleistocene Eurasian continental interior. After Krijgsman et al. (2019), based on maps by Abdullayev et al. (2012) and Vinogradov (1969), respectively. The study location is indicated by the yellow dot, SCB: South Caspian Basin. Dark blue colors represent deep water environments, light blue shallow water (shelf) environments, and orange the large fluvial plains in the Pliocene Productive Series. (For interpretation of the references to colour in this figure legend, the reader is referred to the web version of this article.)

summer monsoon (Ramstein et al., 1997). Therefore, a transition from a series of small endorheic lakes to a large interconnected Paratethyan sea will significantly influence the atmospheric continent-ocean contrast. A large Paratethys sea may further affect the North African monsoon circulations and decreases sensitivity to orbital forcing in this region, prohibiting the oscillation between arid (desert) and humid (green Sahara) periods paced by precession (Zhang et al., 2014).

One of the most extreme changes in Paratethys surface area occurred during the Pliocene-Pleistocene transition interval, with the so-called Akchagylian flooding of the Caspian Basin. During most of the Pliocene, the Black Sea and Caspian basins were endorheic lakes of much smaller size compared to the present-day (Fig. 1a). Coarse-grained deposits of the paleo-Volga delta prograded ~700 km southward into the South Caspian Basin (SCB) to form the main reservoirs of the South Caspian oil province (Abdullayev et al., 2012). This long-term fluvio-deltaic lowstand was rapidly replaced by highstand brackish-marine conditions for much of the Early Pleistocene (e.g. Van Baak et al., 2013). Related to this sea-level rise, the surface area of the Caspian Sea increased fivefold, predominantly over the relatively flat northern shelf region (Fig. 1b), and the Caspian Sea reconnected to the Black Sea, which in turn potentially drained into the Mediterranean (Popov et al., 2006).

Causal mechanisms of the Akchagylian flooding of the Paratethys are still poorly understood and a process-based understanding of the consequences is conspicuously lacking due to a general absence of high-resolution age constraints (Krijgsman et al., 2019). Widely varying age estimates between 4.2 and 1.2 Ma have been proposed and it is currently unknown how this flooding correlates to the global marine record and the terrestrial records of Central Asia (see Van Baak et al., 2013 for details). Here, we combine high-resolution magnetostratigraphy and ^{40}Ar/^{39}Ar geochronology to place the Plio-Pleistocene flooding of the Caspian Basin and its reconnection to the Black Sea into a global framework. We create a basic magnetostratigraphic age model for the Jeirankechmez section in Azerbaijan to place the large scale paleoenvironmental changes, previously documented using micropaleontology and palynology (Richards et al., 2018), in a chronological context. Water fluxes to the Caspian Basin are quantitatively constrained using ^{87}Sr/^{86}Sr ratios. Finally, we discuss the causes and consequences of the major hydrological shift in Central Eurasia occurring during the Plio-Pleistocene transition interval.

2. The Jeirankechmez section

The Plio-Pleistocene flooding of the Caspian Basin can be excellently studied in land-based sections in Azerbaijan. In the Gobustan region,

southwest of the capital Baku, long and complete records of Plio-Pleistocene sediments are exposed in outcrops continuous for several kilometers along strike (Fig. 2). The Jeirankechmez section crops out in a series of interconnected hills, covering a total stratigraphic thickness of ~1600 m on the southeastern flank of an anticline along the Jeirankechmez river (base of the section N40.2378°, E49.3653°).

Lithologically, the lowermost 768 m are characterized by fluvio-deltaic sandstones and brown (silty) clays attributed to the Pliocene Productive Series. This is overlain by > 800 m of light-grey and yellow-brown laminated clays and marls, with faunal elements typical for the Akchagylian and Apsheronian regional stages (Richards et al., 2018). In the fluvio-deltaic deposits, microfauna and palynoflora are generally scarce (Fig. 3). At the initial flooding phase, conditions are characterized by abundant freshwater algae (mainly *Pediastrum* and *Botryococcus*) and ostracods, indicating a fresh-water lacustrine environment (interval 768 to 780 m; see Fig. 3). Predominantly non-forest pollen (e.g. *Artemisia* and Amaranthaceae) suggest cold and dry conditions. Between 780 m and 840 m, a series of over ten volcanic ash layers is present.

A major change occurs in the interval between 784 m and 815 m. This interval is associated with marine indicative dinoflagellate cysts, with a common presence of *Algidasphaeridium* cf. *capillatum* (Richards et al., 2018). Other dinoflagellates include forms such as *Islandinium minutum, Operculodinium centrocarpum* sensu Wall & Dale 1966, and cysts of *Pentapharsodinium dalei*. Furthermore, a distinct assemblage of marine foraminifera is recorded between 798 m and 815 m, including frequent specimens of the calcareous benthonics *Cassidulina* and *Cibicides lobatulus*. Morphometric analyses suggest a close resemblance of the species of *Cassidulina* to *C. reniforme* (Richards et al., 2018). This foraminiferal event during the Akchagylian stage has similarly been documented in biostratigraphic studies in several other regions of the Caspian Sea (Agalarova et al., 1940; Jones and Simmons, 1996 and references therein), and has been interpreted to most likely have originated from the Arctic Ocean (Richards et al., 2018).

The overlying interval c. 819 m until 834 m contains the first appearance (up section) of an assemblage of brackish-water algae (*Pterospermella*), acritarchs (*Mecsekia*) and dinocysts (*Bitectatodinium/Batiacasphaera*), which is the first sign of a typical Caspian Sea and Black Sea association indicative of reduced salinities (Richards et al., 2018). No *Cassidulina* or significant numbers of *Algidasphaeridium* cf. *capillatum* were recorded in this interval, suggesting that the (presumed) marine connection had ceased by this time.

A major change in faunal assemblages occurs at around 836 m (Richards et al., 2018). This level sees a large increase in the numbers of ostracod faunas. Roughly coinciding with this level, fragments of
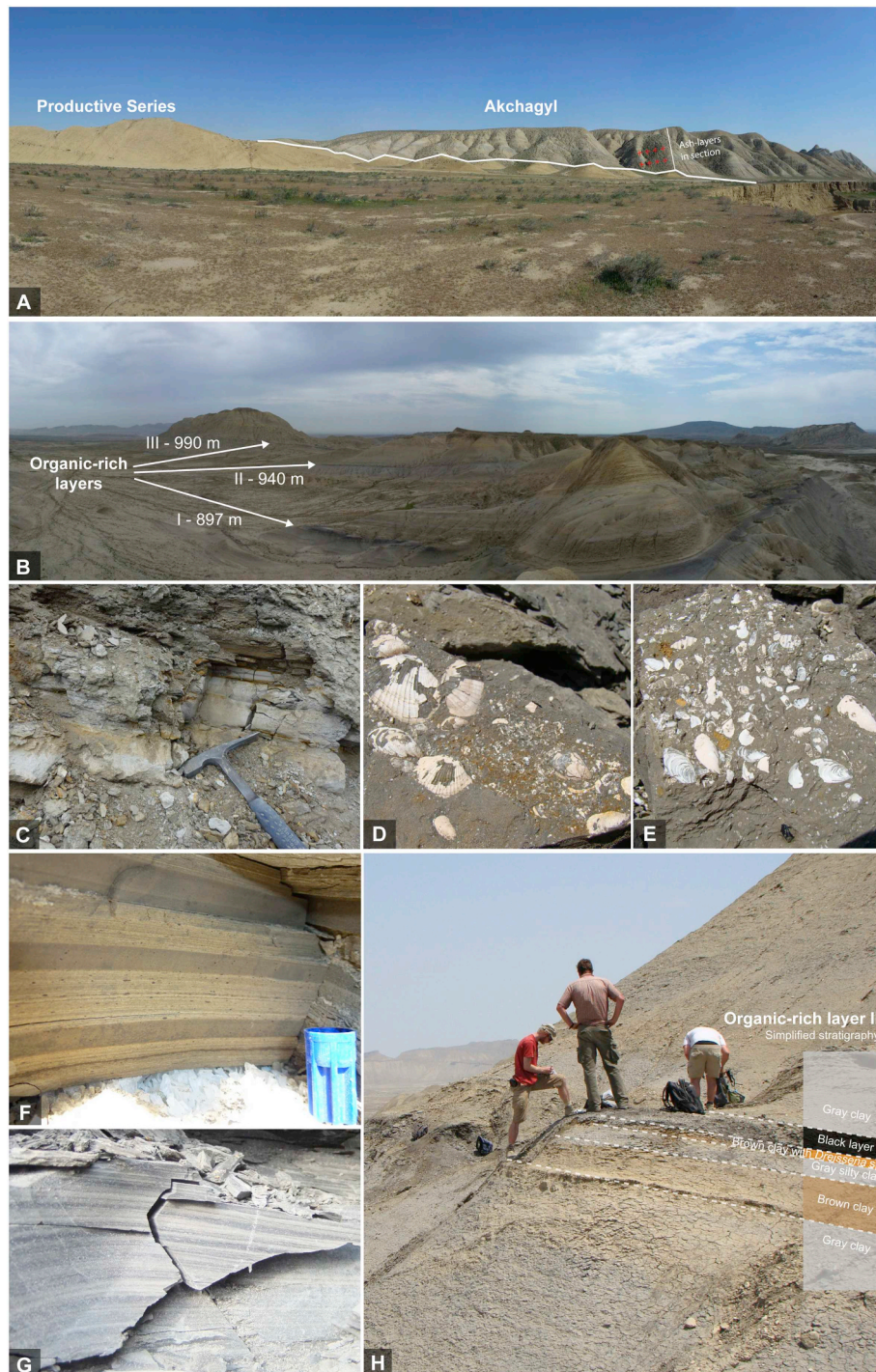
Fig. 2. Field photographs along the upper part of the Jeirankechmez section. a) Interval between 730 and ~800 m across the Productive Series-Akchagyl boundary, b) Overview photograph for the interval 850–1000 m containing the three prominent organic-rich levels, c) Volcanic ash layers (779 m), d,e) Third organic-rich level with abundant mollusc and ostracod fauna, f,g) Very fine laminations in both brown (approx. 800 m) and grey (approx. 850 m) clays, h) The second organic-rich level (940 m) with interpreted stratigraphy. (For interpretation of the references to colour in this figure legend, the reader is referred to the web version of this article.)

Dreissena sp. molluscs start to appear in low numbers. Deposition was predominantly within the brackish realm, indicated by the ostracod faunas which included leptocytherids. From 836 m onwards, the dinocyst assemblages include consistent and sometimes common *Spiniferites 'pannonicus-tihanyensis', Seriliodinium explicatum, Pyxidinopsis psilata* and several species of *Impagidinium*. This assemblage shows similarity with some Black Sea dinocyst records (Mudie et al., 2011 and references therein) and suggests this interval was not subject to fully open marine influences. Relatively stable, but variable, brackish conditions

continue upwards throughout the studied section, indicated both by dinoflagellate cysts and ostracod faunas. At three levels (897 m, 940 m and 990 m), organic-rich (sapropel) layers of up to 1 m thick are found. The third distinctly organic-rich level sees the first abundant mollusc fauna in the section. Higher in the section, molluscs are found both in fossil-rich accumulations, and as individual specimens within the fine grained sediments.

Notable ostracod first consistent appearances from a stratigraphic point of view are *Camptocypria* sp. at 913 m, *Cytherissa bogatschovi*
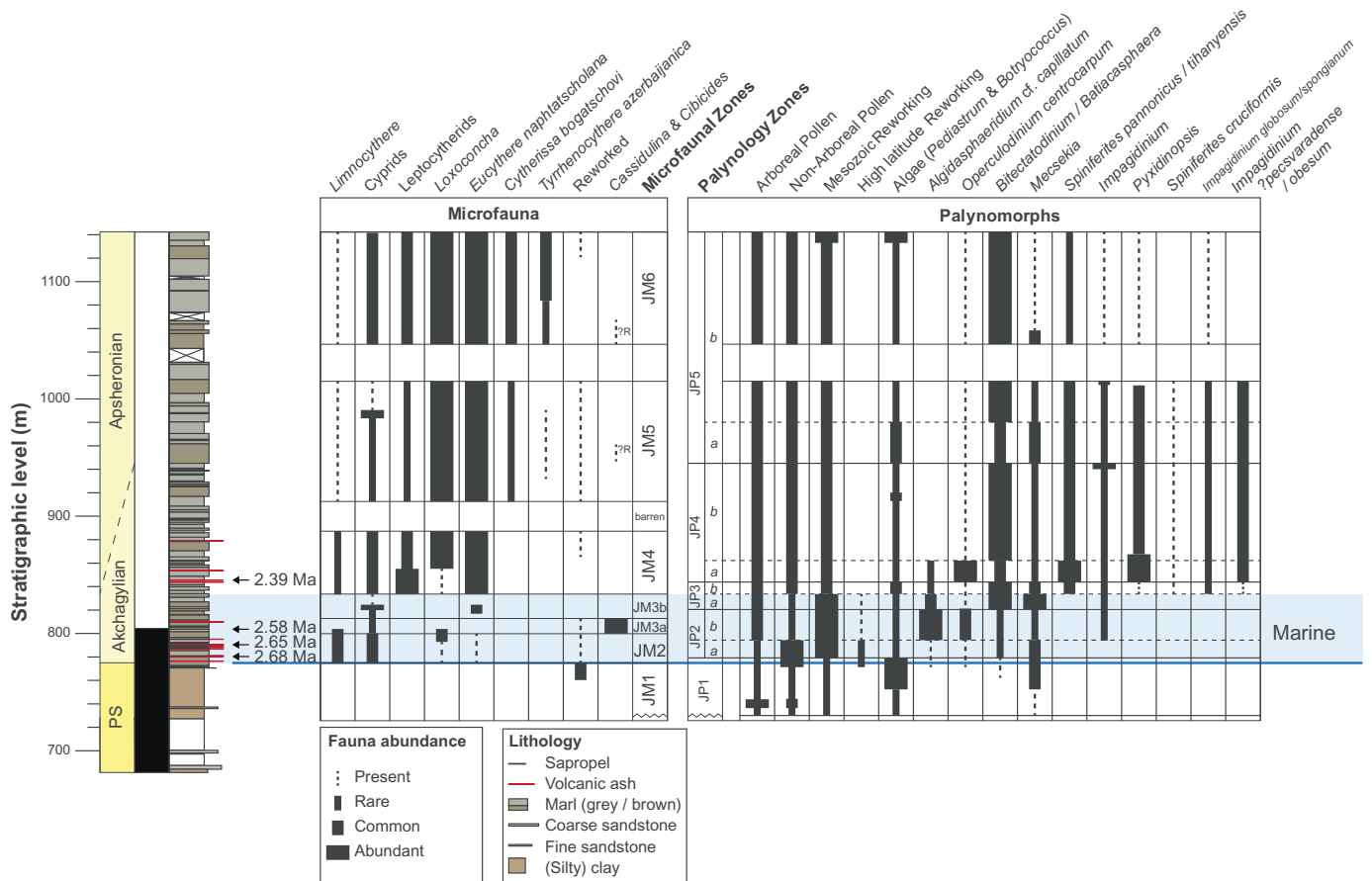
Fig. 3. Summary of biostratigraphic data for the Jeirankechmez section, showing relative abundance changes for the principal ostracod, foraminiferal and palynomorph taxa (Adapted from Richards et al., 2018).

(Livental) at 936 m and *Tyrrhenocythere azerbaijanica* at 1056 m. These ostracod faunas are typical for the Apsheronian stage, although boundary definitions between studies may vary (Krijgsman et al., 2019), making pin-pointing the exact boundary in this succession a difficult exercise (Richards et al., 2018).

3. Dating the Plio-Pleistocene flooding of the Caspian Basin

3.1. Magnetostratigraphy

Paleomagnetic sampling and processing followed standard techniques as described by e.g. Van Baak et al. (2013). 268 levels were sampled with double cores at each level. Paleomagnetic measurements were performed at the paleomagnetic laboratory Fort Hoofddijk of Utrecht University (The Netherlands). Bulk magnetic susceptibility was measured for each specimen on an AGICO MFK1-FA. A total of 217 specimens were thermally demagnetized up to a maximum temperature of 620 °C (typical for the fluvio-deltaic samples) or lower temperatures of max ~400 °C (typical for the Akchagylian and Apsheronian marls), at which point the total magnetization dropped below 10% of the Natural Remanent Magnetization (NRM). The magnetization was measured after each temperature step on a 2G Enterprises DC SQUID cryogenic magnetometer. All demagnetization data and interpretations are available in Appendix A, and can be viewed using the paleomagnetism. org portal (Koymans et al., 2016).

In the lower fluvio-deltaic part the average magnetic susceptibility (over 104 samples) is 3.8×10^{-7} m^3/kg, while in the brackish-marine part this is lower at 8.6×10^{-8} m^3/kg (over 164 samples – Appendix B). Upon thermal demagnetization, 197 samples show a component up to a maximum temperature of 180 °C. Two distinct higher temperature

components of both normal and reverse polarity are observed at higher temperatures, one up to a maximum of 400 °C (Fig. 4a,b), and one up to a maximum of 620 °C (Fig. 4d,e). The in-situ directions of the low temperature (LT) component are oriented in the direction of the geocentric axial dipole (GAD) field expected at this location (inc: 59.3°), indicating this component represents a present-day field overprint of the original signal. For the middle (MT) and high temperature (HT) component, in-situ directions do not coincide with the GAD direction. Instead, the bedding-tilt corrected directions (tc), are concentrated near the north and south axes (Fig. 4c,f). More scatter in the distribution is observed in the MT component compared to the HT component, reflecting the weaker intensities of the samples.

The created magnetostratigraphy shows three normal polarity and two reversed zones between 172 m and 803.5 m, followed by a relatively long reversed polarity interval (Fig. 5). The uppermost 200 m of the section shows predominantly normal directions. Due to the poor continuity of exposure between 1200 and 1400 m, the exact position of the uppermost R/N polarity reversal is unclear.

3.2. ⁴⁰Ar/³⁹Ar geochronology

Within the first 100 m overlying the flooding a series of prominent, white volcanic ash layers is interbedded in the otherwise fine-grained sediment (Fig. 2). Individual ash beds vary in thickness between 1 and 10 cm with thin oxidized edges. The beds are typically massive, without any internal sedimentary structures. In total, 11 volcanic ash layers were sampled for ⁴⁰Ar/³⁹Ar dating.

All samples were disintegrated, washed and sieved over sieves with 63, 90, 250 and 500 μm mesh size. We selected the three best ash layers with the least visible oxidization on the grains from the lower (2BC –
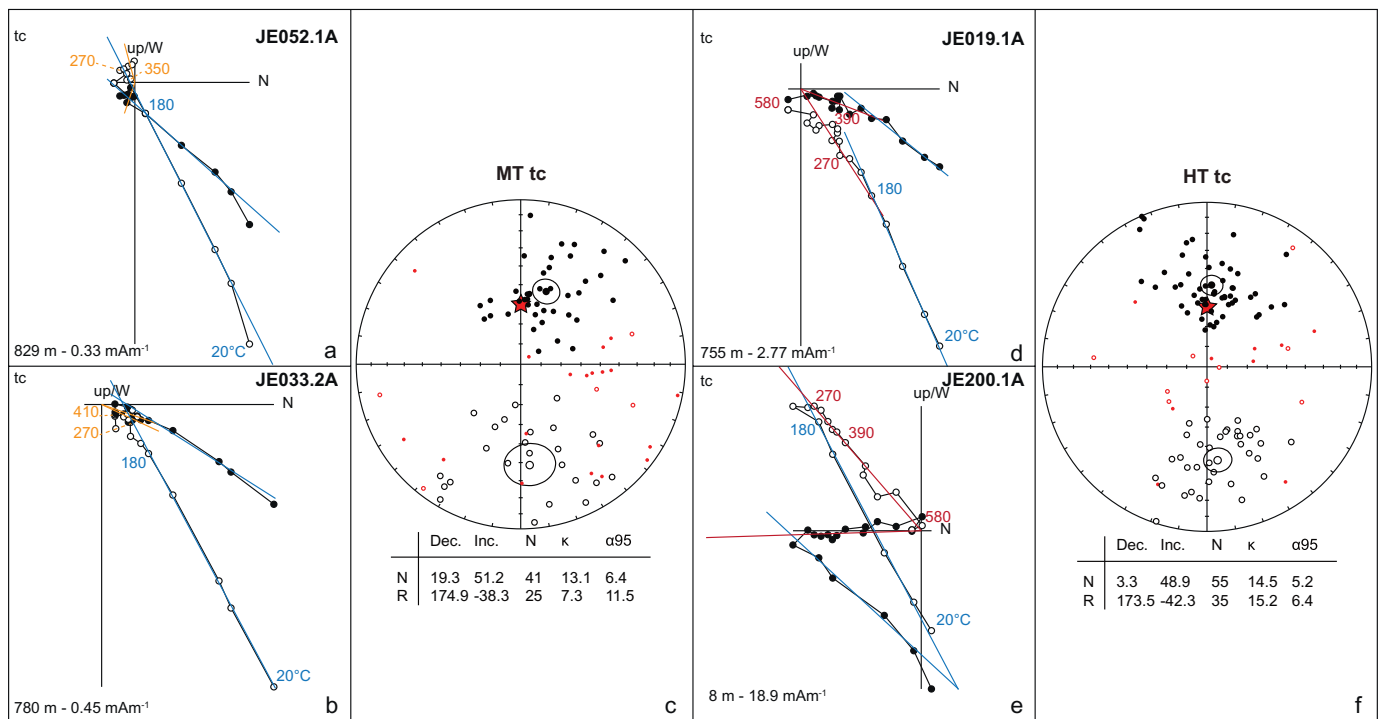
Fig. 4. Typical demagnetization diagrams (all presented up/W), and equal area plots for MT and HT temperature components after tectonic correction (tc). Different colors represent LT (blue), MT (orange) and HT (red) temperature components, temperature is indicated for some steps. Lower left: stratigraphic level and NRM-intensity, top right sample code. a,b) MT reverse and normal, d,e) HT reverse and normal. In the equal area plots (c,f), the red star indicates the GAD direction. Open (closed) circles represent upward (downward) projection, small red dots are direction outside a 45° cut-off. Tables summarize directional components; Dec: declination, Inc.: inclination, N: number of samples, κ: Fischer precision parameter, α95: cone of 95% confidence. Directions are separated in normal (N) and reverse (R). (For interpretation of the references to colour in this figure legend, the reader is referred to the web version of this article.)

779 m), middle (5BC – 788 m) and upper parts (10BC – 852 m) of the ash interval. Heavy liquid separation at densities of 2.54 and 2.59 g/cm^3 produced a poor quality sanidine feldspar fraction, which was not favored for further analysis. Instead, we performed another separation at a higher density (density of 2.92 g/cm^3) on these three ashes on the size fraction between 250 and 500 μm to isolate a biotite fraction. Samples were then leached for one minute in 3% HNO$_3$. Finally, the biotite fraction was handpicked under a microscope. Fish Canyon tuff sanidine (FCs) was used as known standard at an age of 28.201 Ma (Kuiper et al., 2008).

Samples and standards were irradiated for 18 h at the Petten High Flux Reactor (The Netherlands) in the Cd shielded RODEO-P3 position. $^{40}Ar/^{39}Ar$ measurements were performed at Vrije Universiteit Amsterdam (The Netherlands) on a Helix-MC noble gas mass spectrometer. The instrumental setup as used for measuring $^{40}Ar/^{39}Ar$ is explained in Van Baak et al. (2015). Twenty duplicate measurements were performed for each sample (Appendix C). J-values of the samples were for 2BC 0.00444066 ± 0.00001288 (1σ), for 5BC J = 0.00443664 ± 0.00001287 (1σ), and for 10BC J = 0.00443262 ± 0.00001330 (1σ). Neutron interference corrections are $(^{39}Ar/^{37}Ar)_{Ca} = 0.000733 ± 0.000035$, $(^{36}Ar/^{37}Ar)_{Ca} = 0.000265 ± 0.000008$ and $(^{40}Ar/^{39}Ar)_K = 0.001340 ± 0.000787$. The different argon isotopes were measured on H2 - Faraday (m/e 40) and H1 - L2 compact discrete dynodes (CDD; m/e 39-36). Gain correction factors for the different CDDs were determined by measuring mass 44 (CO2) in dynamic mode yielding the following gain factors: 0.9780 ± 0.0040 (1σ) for H1/L2, 1.0006 ± 0.0040 (1σ) for AX/L2 and 1.0152 ± 0.0038 (1σ) for L1/L2. We did not apply a gain correction for the H2-Faraday, but ran all samples, standards and air pipettes consecutively. Bias introduced this way is minor and < 5 ka (e.g. Van Baak et al., 2015). The CO$_2$ signal is too low for the Faraday detector to determine a reliable gain correction factor, but indicates that the gain for H2/L2 is ~0.8959 ± 0.0108. The

resulting correction for the minor incorrectness of the H2/L2 gain is for all samples < 5 kyr too old. For the calculations, decay constants were taken from Min et al. (2000) and the atmospheric air value from Lee et al. (2006). Calculations result in weighted mean ages of 2.68 ± 0.03 Ma (2BC), 2.65 ± 0.04 Ma (5BC) and 2.39 ± 0.05 Ma (10BC), all 1σ (Fig. 6).

3.3. The age of the Akchagylian flooding

The magnetostratigraphic polarity pattern of the Plio-Pleistocene Jeirankechmez section can be straightforwardly correlated with the Geomagnetic Polarity Time Scale (GPTS) 2012 (Hilgen et al., 2012), indicating that the studied record has an age between ~3.8 and ~1.8 Ma (Fig. 5). The interval with three normal and two reversed zones located between 172 m and 803.5 m provides a correlation with the Gauss chron (3.596–2.581 Ma). Section upwards in the marine deposits, the most logical correlation of the upper normal polarity zone assuming continuous deposition is with chron C2n (Olduvai).

The magnetostratigraphic correlation is in excellent agreement with the $^{40}Ar/^{39}Ar$ dating of the three intercalated volcanic ash layers, with 2BC (2.68 Ma) and 5BC (2.65 Ma) located within the upper part of the Gauss chron and 10BC (2.39 Ma) in the lower part of the Matuyama chron. To get to the age of the flooding event, we linearly extrapolate downwards from the age constraints provided by the magnetostratigraphy (2.581 Ma at 803.5 m) and the $^{40}Ar/^{39}Ar$ ages. This way, the age of the Akchagylian flooding level can be estimated to be around 2.7 Ma, which roughly correlates to marine isotope stage (MIS) G6 (Fig. 7).

Another important event is the interval with faunal indications for higher salinity conditions. The first indication of higher salinities in the marine palynology record (784 m) occurs between our lower two dated ash layers, and should therefore date to ~2.67 Ma. The interval with *Cassidulina* foraminifera (797–815 m) should roughly correlate to
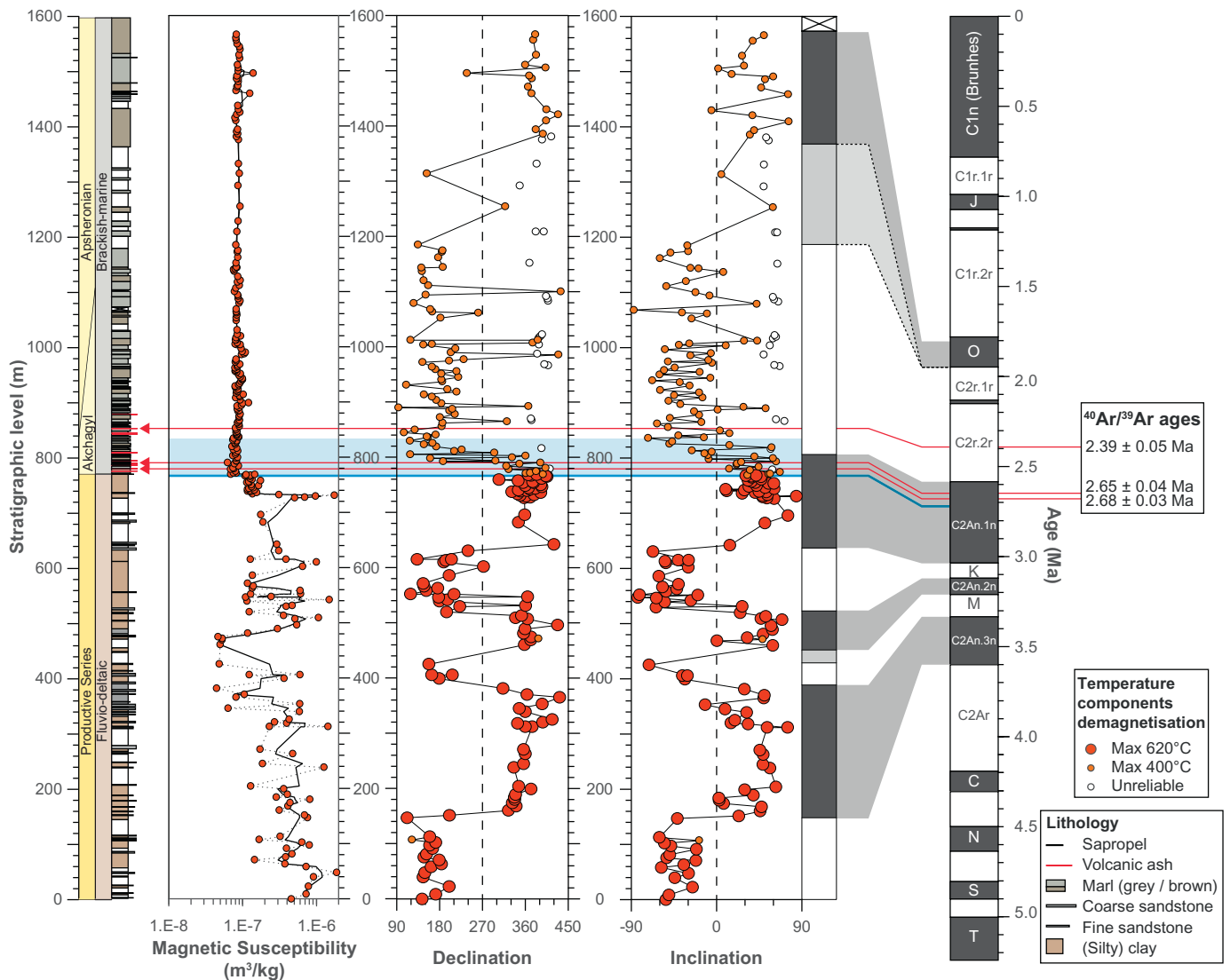
Fig. 5. Magnetostratigraphy and correlation to the GPTS for Jeirankechmez section. From left to right: Lithological record, Specific magnetic susceptibility of the paleomagnetic samples (dashed line average value for Productive Series (3.68×10^{-7} m³/kg) and Akchagyl (8.64×10^{-8} m³/kg), declination, inclination and polarity pattern and correlation to GPTS.

2.5–2.6 Ma. The switch to lower salinity indicative fauna (835 m) pre-dates the ash age of 2.39 Ma (853 m), and may therefore correlate with the interval of isotope stages MIS 100–96 at an age slightly older than 2.4 Ma. The three organic-rich sapropel intervals can be placed in the lowermost Matuyama reverse chron, younger than ash 10BC at 2.39 Ma, but older than the base of chron C2n (Olduvai) at 1.945 Ma. Exact ages for these events are difficult to determine given the uncertainty of the position in our section for the base Olduvai reversal. Similarly, the age of the Akchagylian-Apsheronian regional stage boundary is difficult to assess. However, our data are consistent with a position below the Olduvai chron rather than at the top of the Olduvai chron.

4. The source of the Akchagylian waters

4.1. $^{87}Sr/^{86}Sr$ analyses

To quantitatively assess the potential connectivity changes related to the arrival of marine faunas in the Akchagylian, we measured $^{87}Sr/^{86}Sr$ isotopic composition on ostracods. In semi-isolated basins such as the Paratethyan seas, $^{87}Sr/^{86}Sr$ are very indicative of changing

basin connectivity and changes in riverine input (for details see Vasiliev et al., 2010). All $^{87}Sr/^{86}Sr$ analyses were performed on handpicked ostracod specimens of *Ilyocypris bradyi* and *Caspiocypris*. Strontium isotopic analyses were carried out on a Finningan MAT 262 thermal ionisation mass spectrometer (TIMS) at the Vrije Universiteit Amsterdam (see Klaver et al. (2015) for full analytical details).

Our results indicate that prior to the flooding, $^{87}Sr/^{86}Sr$-ratios are around 0.7077 (Table 1), which is slightly below the ratio for present-day rivers draining the Greater Caucasus (Clauer et al., 2000), indicating a local river signal for our section (Fig. 7; Table 2). After the flooding, $^{87}Sr/^{86}Sr$-ratios show a sustained rise as a result of mixing with water with higher ratios. These quickly surpass the ratio for the present-day Caspian Sea, indicating the additional source needs to be located outside the present-day Caspian drainage basin. Given the marine fossil assemblage in this interval, oceanic water with a ratio between 0.70903 and 0.70909 (Farrell et al., 1995) is the most likely source.

$^{87}Sr/^{86}Sr$-ratios stabilize at around 0.7085 at the end of the marine conditions in the section. In the brackish upper part of the section, $^{87}Sr/^{86}Sr$-ratios notably fluctuate at an increased frequency compared to the preceding interval. Across the three sapropel intervals the
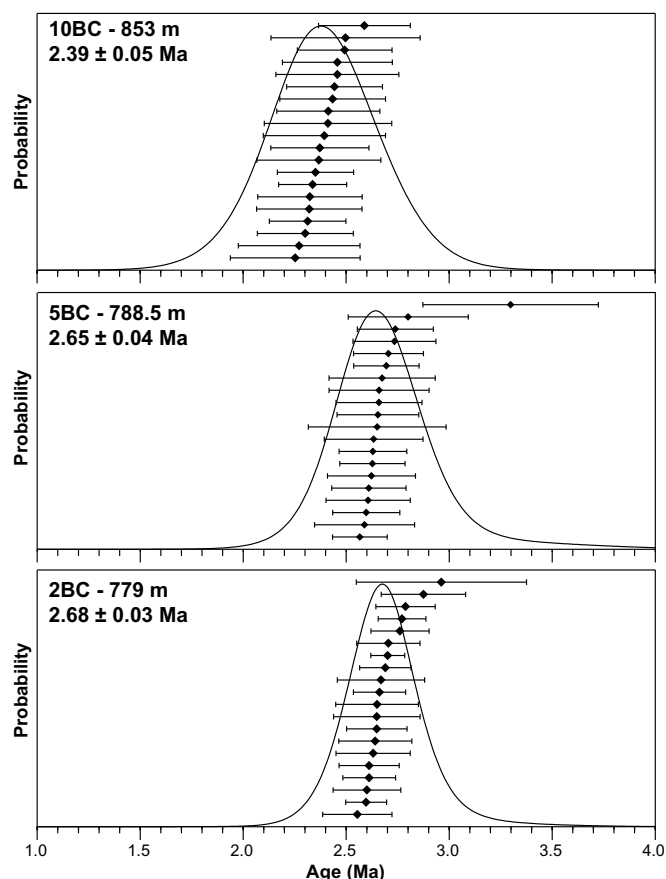
Fig. 6. Probability density diagrams for $^{40}Ar/^{39}Ar$ measurements with all individual analyses and error margins.

$^{87}Sr/^{86}Sr$-ratios increase to values exceeding 0.7087, with subsequent decreases in the intervening intervals. These $^{87}Sr/^{86}Sr$-ratios are similar to the present-day northern rivers of the Black Sea (Don and Dniester) and approach the range of the Last Glacial Maximum (LGM) values for the Black Sea (Major et al., 2006). Therefore, increased connectivity with the Black Sea drainage basin may explain these $^{87}Sr/^{86}Sr$-ratios. However, to compensate for the low Volga ratio of 0.70802 which constitutes about 80% of all riverine input into the present-day Caspian, an additional high-ratio source is needed for the observed stable values. Whether this should be interpreted as an oceanic component unnoticed in the fossil record, or in terms of another, unknown, source of riverine input, is beyond the scope of the current study.

4.2. Indications for an Arctic connection

The marine fossil fauna found at the Jeirankechmez section between 797 and 815 m indicate that a marine connection may have existed between the Arctic Ocean and the Caspian Sea (Richards et al., 2018). Although this may seem like an extreme hypothesis, close biological and hydrological connections between the Caspian Sea and the Arctic Ocean have been documented in the past. In fact, marine species with an Arctic origin can be found in the present-day Caspian Sea. Some of these species, like the currently endangered land-locked Caspian seal (*Pusa caspica*), have been linked to an enigmatic introduction during the Plio-Pleistocene (Palo and Väinölä, 2006).

The marine foraminifera that are found in the Jeirankechmez section, particularly *Cassidulina*, are indicative for cold waters (Sejrup and Guilbault, 1980), and show that the Caspian Sea intermittently received marine water from the open ocean during the Plio-Pleistocene transition (Richards et al., 2018). Neither *Cassidulina* nor *Cibicides lobatulus*

occur in the Caspian Sea at present time, and have not been recorded there in the more recent Pleistocene. Species of *Cassidulina* occur at the present time in the Marmara Sea (Kaminski et al., 2002), but not in the Black Sea (Yanko, 1990). *Cibicides lobatulus*, however, is known from the Black Sea but not from the Caspian Sea in the recent geological past (Yanko, 1990). Finally, we note the frequent occurrences of *Algidasphaeridium* cf. *capillatum*. This is essentially a high-latitude northern hemisphere form (Matsuoka and Bujak, 1988), and would support the interpretation of a northern marine connection between the Arctic Ocean and the Caspian Sea.

Here we date this marine interval, and show that after the flooding at around 2.7 Ma, peak marine conditions occurred between 2.5 and 2.6 Ma. In time, this closely correlates with the first major late Pliocene expansion of Scandinavian ice sheets (De Schepper et al., 2014) suggesting climatic changes in or near the northern Paleo-Volga drainage area may have played an important role in the Caspian Sea region. For instance, it is possible that the Scandinavian ice sheet entered the Paleo-Volga drainage at this time. Similar intermittent hydrological connections between the Arctic region and the Caspian Sea have previously been proposed for the late Pleistocene, related to dynamic surface lowering and the formation of large ice-dammed lakes forming in front of continental ice sheets penetrating the Caspian catchment area (Mangerud et al., 2004). Fresh glacial meltwater would increase the Caspian water budget, although this would predominantly be significant on short time scales. It also does not explain the increased salinities we find in our Caspian Sea record at this time. Dynamic topographic lowering related to ice loading caused by the continental glaciations would be an additional factor which may be important to the formation of an Arctic-Caspian marine passage at the end of the Pliocene.

The present-day northern boundary of the Volga drainage is largely formed by the topography of Late Pleistocene ice-drift limits at ~60°N (Fig. 8). Eliminating this younger topographic barrier would increase the size of the late Pliocene Palaeo-Volga drainage towards the north. In addition, a major, up to 600 m deep incised canyon system of the Palaeo-Volga river was still present at this time (Sidnev, 1985; Kroonenberg et al., 2005). At present this has been completely filled up with younger sediments (in particular of Akchagylian and Apsheronian age), but at the time this was a major erosive structure at the scale of the Grand Canyon cutting its way in a north-south direction deep into the Russian Plain. This would have greatly benefitted the creation of a long distance water pathway across the continent.

The end of marine conditions and the establishment of long-term brackish conditions in our record prior to 2.4 Ma suggests that related to the glacial maxima of MIS100–96, the oceanic influx(es) into the Caspian Sea terminated. This mechanism would also explain why at this time the marine conditions in the Caspian Sea were lost. After isotope stages MIS 100, 98 and 96, the following time period is globally characterized by more stable warmer conditions, including a number of long super-interglacials (Brigham-Grette et al., 2013). The lack of large Scandinavian ice sheets would have prevented the Arctic-Caspian passage from reopening. Instead, in the subsequent warm period, our data suggests that connectivity with the Black Sea became increasingly important for the environmental conditions in the Caspian Sea.

5. Paleoenvironmental impact

5.1. Eurasian continental hydrology across the iNHG

The Caspian Sea drainage basin plays an important role in the paleoenvironmental evolution of Central Eurasia. At present, the Volga river supplies > 80% of the total water flux into the Caspian Sea and its discharge is regulated by precipitation variations in the high northern latitudes. Long rivers like the Volga, but also the Amu Darya and Syr Darya transport water for 1000's of kilometers, and allow for climatic processes of the high northern latitudes and even the Pamir and
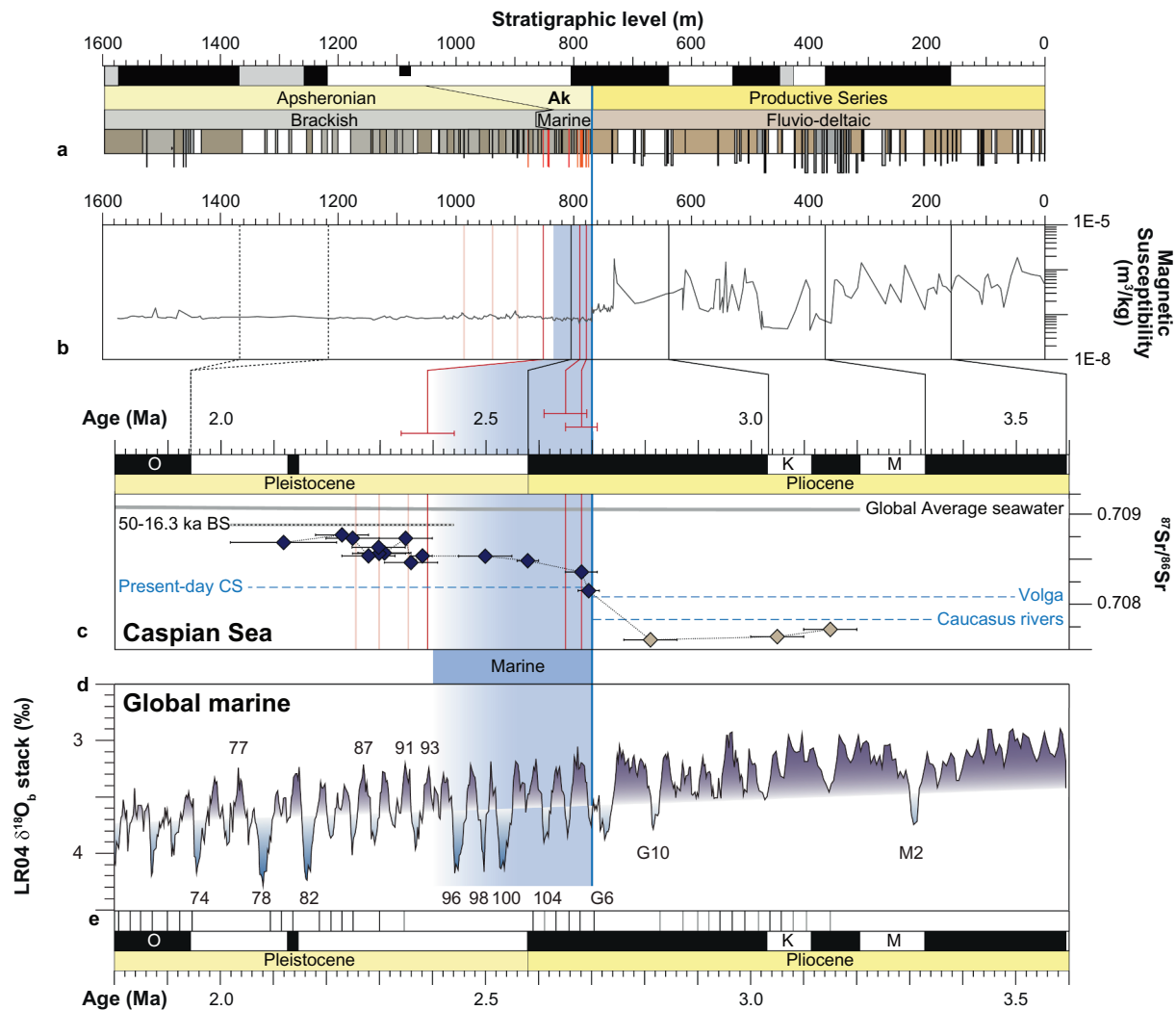
Fig. 7. The Jeirankechmez record and correlation to global records. a) Magnetostratigraphy and lithological record, and b) Specific magnetic susceptibility. Both records are plotted against stratigraphic level, blue vertical line represents the flooding and the interval with marine conditions as observed in the fossil record. In brown between 900 and 1000 m the three sapropel levels. Red lines indicate the $^{40}Ar/^{39}Ar$ ages of the volcanic ashes, including uncertainties, in black magnetic reversals. All subsequent plots are plotted in the time domain. c) $^{87}Sr/^{86}Sr$ ratios of the Jeirankechmez section. Dashed horizontal blue lines indicate present-day $^{87}Sr/^{86}Sr$-ratios for Caspian Sea and rivers, in grey Plio-Pleistocene global average seawater (see Tables 1 and 2 for values and references). d) Global benthic $\delta^{18}O$ stack with major glacial stages indicated (Lisiecki and Raymo, 2005). e) Timing of Mediterranean sapropels (Kroon et al., 1998). (For interpretation of the references to colour in this figure legend, the reader is referred to the web version of this article.)

Himalaya mountains to contribute to the variability of the Caspian hydrological budget (Fig. 1). Our new chronologic results allow an integration between the continental paleohydrology of Eurasia and the global climatic changes of the late Pliocene. We show that the fivefold increase in the size of the Caspian Sea is related to the global climatic cooling step at 2.7 Ma, and that the size of the Caspian Sea during the early Pleistocene remained significantly larger compared to the Pliocene stable state. This indicates, in addition to a potential short marine connection, a link to large-scale shifting precipitation patterns across the Eurasian continent between the Pliocene and Pleistocene.

The expansion of the Caspian Sea at the end of the Pliocene should be seen as an important part of changing continental climate across Eurasia around 2.7 Ma. Concurrent shifts have previously been recorded, most notably drying in the Eurasian high latitudes (Brigham-Grette et al., 2013), and the onset of cyclic Chinese Loess deposits (e.g. Sun et al., 2006). The variations in the composition of the Chinese Loess have been correlated to climate events in the North Atlantic through changing patterns in westerly winds (e.g., Maher, 2016). Similarly, these play an important role in the hydrological budget of the Caspian Sea by supplying moisture from the North Atlantic into the Volga

drainage. The North Atlantic-derived moisture, which no longer was supplied by western winds to the high northern latitudes (Brigham-Grette et al., 2013), may have been delivered further south, allowing the Caspian Sea to experience long-term stable high-stand conditions during the early Pleistocene. Loess records close to the Caspian Sea in northeastern Iran, which are interpreted to represent climate conditions wetter than at present, similarly suggest an increased humidity locally around the Caspian Sea (Wang et al., 2016). These loess deposits are notably underlain by undated shallow water Akchagylian marine sediments. This is consistent with our new 2.7–2.4 Ma age for the Akchagylian marine phase.

5.2. Potential impact of Paratethys on ocean circulation patterns

Although marine in salinity, the Mediterranean Sea is a semi-isolated basin highly susceptible to changes in hydrological budget (Marzocchi et al., 2016). Constraining the long-term variability of fresh water coming off the Eurasian continent is therefore crucial. The typical effect of enhanced fresh-water supply to the Mediterranean Sea is stratification and the formation of organic-rich sapropels. While poorly

Table 1
Sr isotope results and details.

Stratigraphic level (m)	Sample code	Regional stage	Species	$^{87}Sr/^{86}Sr \pm$ 2 SE	Age (Ma)	Age error (Ma)	Comment
512.7	JE 163.2	Productive Series	*Ilyocypris bradyi*	0.707722 ± 12	3.15	0.05	
614.8	JE 153	Productive Series	*Ilyocypris bradyi*	0.707642 ± 9	3.05	0.05	
726.0	JE 01	Productive Series	*Ilyocypris bradyi*	0.707607 ± 12	2.81	0.05	
731.5	JE 05	Productive Series	*Ilyocypris bradyi*		2.8	0.05	
771.5	JE29	Akchagylian	*Caspiocypris*	0.708151 ± 9	2.7	0.02	
789.8	JE36	Akchagylian	*Caspiocypris*	0.708358 ± 9	2.65	0.02	
802.4	JE41	Akchagylian	*Caspiocypris*	0.708483 ± 9	2.58	0.02	
825.5	JE 49	Akchagylian	*Caspiocypris*	0.708533 ± 10	2.5	0.05	
840.5	JE58	Akchagylian	*Caspiocypris*		2.45	0.05	
864.6	JE67	Akchagylian	*Caspiocypris*	0.708536 ± 8	2.4	0.05	
892.0	JE77	Akchagylian	*Caspiocypris*	0.708463 ± 7	2.36	0.05	Pre organic-rich level I
903.4	JE80	Akchagylian	*Caspiocypris*	0.708731 ± 9	2.35	0.05	Post organic-rich level I
930.8	JE92	Akchagylian	*Caspiocypris*	0.708569 ± 7	2.31	0.05	
939.6	JE95B	Akchagylian	*Caspiocypris*	0.708564 ± 8	2.3	0.05	Organic-rich level II
944.8	JE98	Akchagylian	*Caspiocypris*	0.708632 ± 10	2.29	0.05	
961.5	JE105	Akchagylian	*Caspiocypris*	0.708537 ± 8	2.28	0.05	
967.9	JE108	Akchagylian	*Caspiocypris*		2.27	0.05	
985.3	JE112	Akchagylian	*Caspiocypris*	0.708732 ± 9	2.25	0.05	Pre organic-rich level III
1003.5	JE118	Akchagylian	*Caspiocypris*	0.708769 ± 9	2.23	0.05	Post organic-rich level III
1093.8	JE137	Akchagylian	*Caspiocypris*	0.708685 ± 9	2.12	0.1	

understood, low salinity water derived from the Eurasian continent contributes towards reducing Mediterranean salinity (Rohling et al., 2015).

Since the Middle Miocene, the Paratethys region, or parts thereof, regularly connected and disconnected from the Mediterranean Sea (Palcu et al., 2017; Sant et al., 2017; Van Baak et al., 2017). The current connection between the Mediterranean Sea and the Black Sea across the Bosporus, and isolation of the Caspian Sea is therefore not necessarily representative for basin connectivity in the past. By including the Caspian drainage, the size of the northern drainage of the Mediterranean Sea would triple in size compared to present. Even under otherwise stable climate conditions, such changes in basin connectivity may drive a non-linear response in adjacent basins.

A marked deep water cooling step around 2.7 Ma was recently proposed for the Mediterranean (Rohling et al., 2014), but this is inferred from techniques not independent of water salinity. At the same time, the prominent sapropel cluster A, starting at 2.70 Ma, highlights increased sapropel activity compared to the Pliocene (Hilgen, 1991). An additional high-latitude component in the Mediterranean sapropel record is present from this time onwards as well, also indicating the increasing importance of the northern influence on the Mediterranean (paleo) hydrology and circulation (Kroon et al., 1998). Here we show that these changes in the Mediterranean coincide with a switch to a more positive hydrological budget and the increased availability of

water on the Eurasian continent. This supports our notion that connectivity between Mediterranean and Atlantic may not be the only important gateway to consider when interpreting the Mediterranean paleoceanography and that (part of) the Mediterranean variability may need to be explained as a connectivity change related to increased freshwater supply directly from the Eurasian continent.

The best studied sapropel in terms of impacts and forcing mechanisms is the Holocene sapropel S1 (Rohling et al., 2015). The effects of sapropel S1 can be traced throughout the Mediterranean, and is represented by a period of disrupted exchange in the Strait of Gibraltar and reduced Mediterranean Outflow Water (MOW) (Rogerson et al., 2012). The MOW can be traced far into the North Atlantic and is a key contributor to the strength and stability of the Atlantic Meridional Overturning Circulation (AMOC), and therefore northern hemisphere climate (Rogerson et al., 2012; Hernandez-Molina et al., 2014). The Gibraltar exchange acts as a negative feedback mechanism to AMOC (Rogerson et al., 2012). MOW strength depends on the Atlantic-Mediterranean density contrast and therefore on fresh water supply to the Mediterranean. Lowering the Mediterranean salinity decreases the density contrast, causing the Mediterranean outflow to become less efficient. As a result, an enhanced Eurasian discharge towards the Mediterranean Sea could potentially have far-reaching effects and decrease the stability of the AMOC.

Table 2
Present-day and paleo Sr isotope ratios for rivers and seas relevant to the study.

| Water body	Sr (ppm)	$^{87}Sr/^{86}Sr$	Reference
Ocean water (modern)	7.62	0.709155	Henderson et al. (1994)
Black Sea (modern)		0.709133	Major et al. (2006)
Aegean Sea (modern)		0.709157	Major et al. (2006)
Marmara Sea (modern)		0.70915	Major et al. (2006)
Caspian Sea (modern)	9.92	0.708183	Clauer et al. (2000)
Volga (modern)	0.48	0.708083	Clauer et al. (2000)
Caucasus rivers (modern)	1.65	0.707795	Clauer et al. (2000)
Southern Caspian rivers (modern)	0.85	0.708293	Clauer et al. (2000)
Don (modern)	0.22	0.7085	Palmer and Edmond (1989)
Dnieper (modern)	0.22	0.7085	Palmer and Edmond (1989)
Black Sea river average (modern)	0.24	0.708792	Major et al. (2006)
Ocean water (Plio-Pleistocene)		0.70903–0.70909	Farrell et al. (1995)
Dacian Basin (Late Miocene-Early Pliocene)		0.708511–0.708964	Vasiliev et al. (2010)
Black Sea (LGM)		0.70865–0.70875	Major et al. (2006)
Black Sea (130–134 ka)		0.7091–0.70945	Wegwerth et al. (2014)
Black Sea (127.5–129.5 ka)		0.7089–0.7091	Wegwerth et al. (2014)
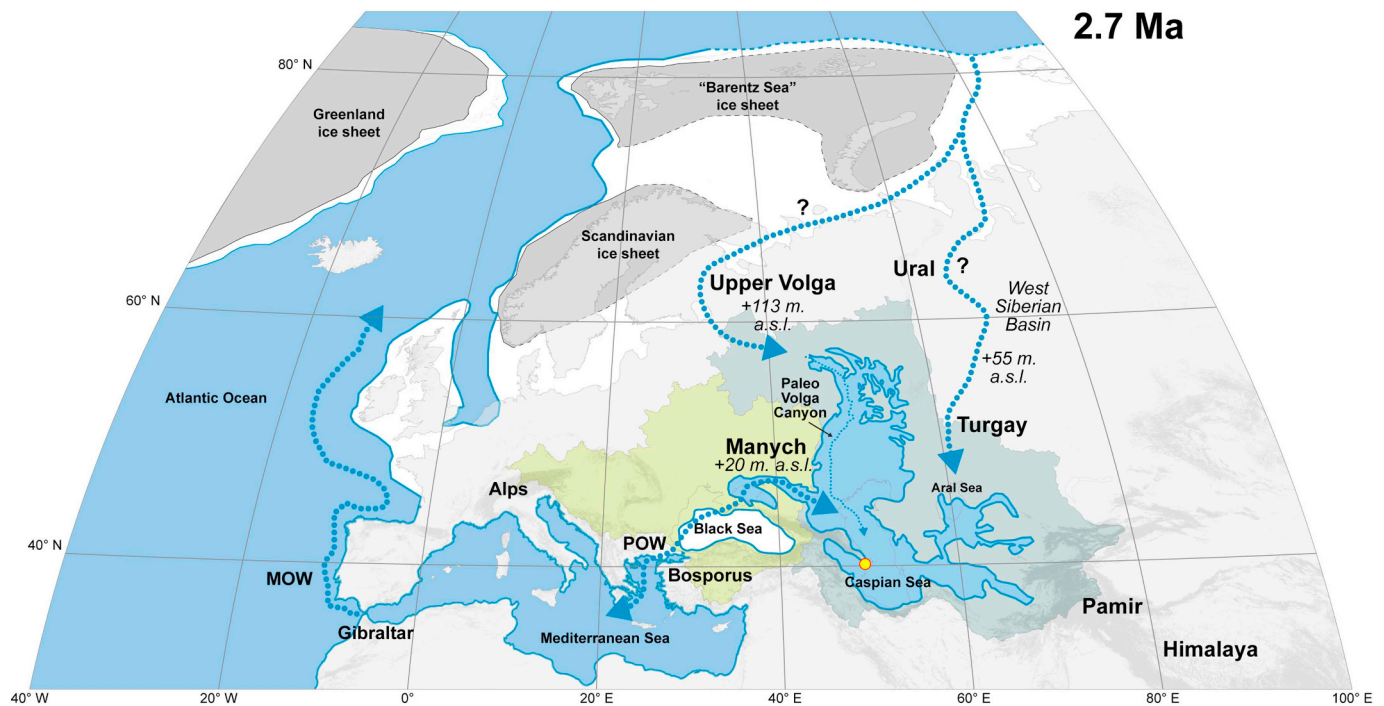
Fig. 8. Paleogeographic map of Eurasia at ~2.7 Ma during the intensification of Northern Hemisphere Glaciations. Indicated are potential marine gateways with the minimum present-day elevation which needs to be crossed to enter the Caspian drainage. In yellow and grey the present-day Black Sea and Caspian Sea drainages. The yellow dot indicates the location of the Jeirankechmez section. In light grey the likely extend of the Scandinavian and Barentz ice sheets, dashed lines indicating uncertain positions. Caspian reconstruction after Vinogradov (1969). (For interpretation of the references to colour in this figure legend, the reader is referred to the web version of this article.)

6. Conclusion

The water level of the Caspian Sea, the biggest lake on Earth, acts distinctly out of phase compared to the open ocean sea level. We show that the intensification of Northern Hemisphere Glaciations around 2.7 Ma coincided with a major water level increase in the Caspian Sea. A marine connection to the Caspian Sea may have existed between 2.7 Ma and 2.4 Ma, after which a lowering of the salinity in the Caspian Sea occurred. During the early Pleistocene, the Caspian Sea remained a significantly larger water body compared to the Pliocene. The switch from a small endorheic basin in the Pliocene to a significantly larger sea during the Pleistocene suggests a more positive hydrological budget for the Eurasian continental interior from this time onwards. Changes in the outflow of freshened Paratethys water may have triggered far-field effects in the Mediterranean Sea, forming a previously overlooked positive feedback towards climatic cooling.

The sea-level and connectivity variability of the Paratethyan epicontinental seas on the Eurasian continental interior is a potentially important but poorly understood and overlooked part of the paleoclimatic system. Since the individual Paratethyan sub-basins are separated by shallow sills in tectonically active regions, ultimately regional tectonics may actively contribute to large scale climatic processes by modifying marine connectivity between these basins. Therefore, a variable Paratethys surface area based on accurately dated, regional data, should be included in global climate models describing (continental) climatic variability.

Appendix A. Supplementary data

Supplementary data associated with this article can be found in the online version, at https://doi.org/10.1016/j.gloplacha.2019.01.007. These data include the Google map locations of all sample levels described in this article.

References

Abdullayev, N.R., Riley, G.W., Bowman, A.P., 2012. Regional controls on lacustrine sandstone reservoirs: the pliocene of the South Caspian Basin. In: Baganz, O.W., Bartov, Y., Bohacs, K., Nummedal, D. (Eds.), Lacustrine Sandstone Reservoirs and Hydrocarbon Systems, pp. 71–98. https://doi.org/10.1306/13291385M953446.

Agalarova, D.A., Jafarov, D.I., Khalilov, D.M., 1940. In: Institute, A.O.R (Ed.), Handbook of Microfauna: Tertiary Deposits of the Apsheron Peninsula (in Russian). Azgostoptehizdat, Baku, pp. 54–55.

Brigham-Grette, J., Melles, M., Minyuk, P., Andreev, A., Tarasov, P., DeConto, R., Koenig, S., Nowaczyk, N., Wennrich, V., Rosén, P., Haltia, E., Cook, T., Gebhardt, C., Meyer-Jacob, C., Snyder, J., Herzschuh, U., 2013. Pliocene warmth, polar amplification, and stepped Pleistocene cooling recorded in NE Arctic Russia. Science 340, 1421–1427. https://doi.org/10.1126/science.1233137.

Clauer, N., Chaudhuri, S., Toulkeridis, T., Blanc, G., 2000. Fluctuations of Caspian Sea level: Beyond climatic variations? Geology 28, 1015–1018.

De Schepper, S., Gibbard, P.L., Salzmann, U., Ehlers, J., 2014. A global synthesis of the marine and terrestrial evidence for glaciation during the Pliocene Epoch. Earth-Sci. Rev. 135, 83–102. https://doi.org/10.1016/j.earscirev.2014.04.003.

Farrell, J.W., Clemens, S.C., Gromet, L.P., 1995. Improved chronostratigraphic reference curve of late Neogene seawater 87Sr/86Sr. Geology 23, 403–406. https://doi.org/10.1130/0091-7613(1995)023<0403.

Grothe, A., Sangiorgi, F., Brinkhuis, H., Stoica, M., Krijgsman, W., 2018. Migration of the dinoflagellate Galeacysta etrusca and its implications for the Messinian Salinity Crisis. Newsl. Stratigr 51, 73–91. https://doi.org/10.1127/nos/2016/0340.

Henderson, G.M., Martel, D.J., O'Nions, R.K., Shackleton, N.J., 1994. Evolution of seawater 87Sr/86Sr over the last 400 ka: the absence of glacial/interglacial cycles. Earth Planet. Sci. Lett 128, 643–651.

Hernandez-Molina, F.J., Stow, D.A.V., Alvarez-Zarikian, C.A., Acton, G., Bahr, A., Balestra, B., Ducassou, E., Flood, R., Flores, J.-A., Furota, S., Grunert, P., Hodell, D.,

Jimenez-Espejo, F., Kim, J.K., Krissek, L., Kuroda, J., Li, B., Llave, E., Lofi, J., Lourens, L., Miller, M., Nanayama, F., Nishida, N., Richter, C., Roque, C., Pereira, H., Sanchez Goni, M.F., Sierro, F.J., Singh, A.D., Sloss, C., Takashimizu, Y., Tzanova, A., Voelker, A., Williams, T., Xuan, C., 2014. Onset of Mediterranean outflow into the North Atlantic. Science 344, 1244–1250. https://doi.org/10.1126/science.1251306.

Hilgen, F.J., 1991. Astronomical calibration of Gauss to Matuyama sapropels in the Mediterranean and implication for the Geomagnetic Polarity Time Scale. Earth Planet. Sci. Lett 104, 226–244.

Hilgen, F.J., Lourens, L.J., Van Dam, J.A., 2012. The Neogene period. In: Gradstein, F.M., Ogg, J.G., Schmitz, M.D., Ogg, G.M. (Eds.), The Geological Time Scale 2012. Elsevier BV, Amsterdam, pp. 947–1002.

Jones, R.W., Simmons, M.D., 1996. A review of the stratigraphy of eastern Paratethys (Oligocene-Holocene). Bull. Nat. Hist. Mus. (Geol. Suppl.) 52, 25–49.

Kaminski, M.a., Aksu, A., Box, M., Hiscott, R.N., Filipescu, S., Al-Salameen, M., 2002. Late Glacial to Holocene benthic foraminifera in the Marmara Sea: implications for Black Sea–Mediterranean Sea connections following the last deglaciation. Mar. Geol. 190, 165–202. https://doi.org/10.1016/S0025-3227(02)00347-X.

Klaver, M., Djuly, T., De Graaf, S., Sakes, A., Wijbrans, J., Davies, G., Vroon, P., 2015. Temporal and spatial variations in provenance of Eastern Mediterranean Sea sediments: implications for Aegean and Aeolian arc volcanism. Geochim. Cosmochim. Acta 153, 149–168. https://doi.org/10.1016/j.gca.2015.01.007.

Koymans, M.R., Langereis, C.G., Pastor-Galán, D., Van Hinsbergen, D.J.J., 2016. Paleomagnetism.org: an online multi-platform open source environment for paleomagnetic data analysis. Comput. Geosci. 93, 127–137.

Krijgsman, W., Stoica, M., Vasiliev, I., Popov, V.V., 2010. Rise and fall of the Paratethys Sea during the Messinian Salinity Crisis. Earth Planet. Sci. Lett 290, 183–191.

Krijgsman, W., Tesakov, A., Yanina, T., Lazarev, S., Danukalova, G., Van Baak, C.G.C., Agustí, J., Alçiçek, M.C., Aliyeva, E., Bista, D., Bruch, A., Büyükmeriç, Y., Bukhsianidze, M., Kroonenberg, S.B., Lordkipanidze, D., Oms, O., Rausch, L., Singarayer, J., Stoica, M., 2019. Quaternary time scales for the Pontocaspian domain: interbasinal connectivity and faunal evolution. Earth-Sci. Rev 188, 1–40. https://doi.org/10.1016/j.earscirev.2018.10.013.

Kroon, D., Alexander, I., Little, M., Lourens, L.J., Matthewson, A., Robertson, A.H.F., Sakamoto, T., 1998. Oxygen isotope and sapropel stratigraphy in the Eastern Mediterranean during the last 3.2 milloin years. In: Robertson, A.H.F., Emeis, K.C., Richter, C., Camerlenghi, A. (Eds.), Proceedings of the Ocean Drilling Program, Scientific Results. 160. pp. 181–189.

Kroonenberg, S.B., Simmons, M.D., Alekseevski, N.I., Aliyeva, E., Allen, M.B., Aybulatov, D.N., Baba-Zadeh, A., Babyukova, E.N., Davies, C.E., Hinds, D.J., Hoogendoorn, R.M., Huseynov, D., Ibrahimov, B., Mamedov, P., Overeem, I., Rusakov, G.V., Suleymanova, S.F., Svitoch, A.A., Vincent, S.J., 2005. Two deltas, one basin, one river, one sea: the modern Volga delta as an analogue of the Neogene Productive Series, South Caspian Basin. In: Giosan, L., Bhattacharya, J.P. (Eds.), SEPM Special Publication: River Deltas – Concepts, Models and Examples. SEPM, Tulsa, Oklahoma, U.S.A., pp. 231–256.

Kuiper, K.F., Deino, A., Hilgen, F.J., Krijgsman, W., Renne, P.R., Wijbrans, J.R., 2008. Synchronizing rock clocks of Earth history. Science 320, 500–504.

de la Vara, A., van Baak, C.G.C., Marzocchi, A., Grothe, A., Meijer, P.T., 2016. Quantitative analysis of Paratethys sea level change during the Messinian Salinity Crisis. Mar. Geol 379. https://doi.org/10.1016/j.margeo.2016.05.002.

Lee, J.-Y., Marti, K., Severinghaus, J.P., Kawamura, K., Yoo, H.-S., Lee, J.B., Kim, J.S., 2006. A redetermination of the isotopic abundances of atmospheric Ar. Geochim. Cosmochim. Acta 70, 4507–4512. https://doi.org/10.1016/j.gca.2006.06.1563.

Lisiecki, L.E., Raymo, M.E., 2005. A Pliocene-Pleistocene stack of 57 globally distributed benthic D18O records. Paleoceanography 20, PA1003. https://doi.org/10.1029/2004PA001071.

Maher, B.A., 2016. Palaeoclimatic records of the loess/palaeosol sequences of the Chinese Loess Plateau. Quat. Sci. Rev 154, 23–84. https://doi.org/10.1016/j.quascirev.2016.08.004.

Major, C.O., Goldstein, S.L., Ryan, W.B.F., Lericolais, G., Piotrowski, A.M., Hajdas, I., 2006. The co-evolution of Black Sea level and composition through the last deglaciation and its paleoclimatic significance. Quat. Sci. Rev 25, 2031–2047.

Mangerud, J., Jakobsson, M., Alexanderson, H., Astakhov, V., Clarke, G.K.C., Henriksen, M., Hjort, C., Krinner, G., Lunkka, J.-P., Möller, P., Murray, A., Nikolskaya, O., Saarnisto, M., Svendsen, J.I., 2004. Ice-dammed lakes and rerouting of the drainage of northern Eurasia during the Last Glaciation. Quat. Sci. Rev 23, 1313–1332.

Marzocchi, A., Flecker, R., Van Baak, C.G.C., Lunt, D.J., Krijgsman, W., 2016. Mediterranean outflow pump: an alternative mechanism for the Lago-mare and the end of the Messinian Salinity Crisis. Geology 44, 1–4. https://doi.org/10.1130/G37646.1.

Matsuoka, K., Bujak, J.P., 1988. Cenozoic dinoflagellate cysts from the Navarin Basin, Norton Sound and St. George Basin, Bering Sea. Bulletin Faculty of Liberal Arts, Nagasaki University. Nat. Sci. 29, 1–147.

Min, K., Mundil, R., Renne, P.R., Ludwig, K.R., 2000. A test for systematic errors in 40Ar/39Ar geochronology through comparison with U/Pb analysis of a 1.1-Ga rhyolite. Geochim. Cosmochim. Acta 64, 73–98.

Mudie, P.J., Leroy, S.A.G., Marret, F., Gerasimenko, N., Kholeif, S.E.A., Sapelko, T., Filipova-Marinova, M., 2011. Nonpollen Palynomorphs: Indicators of Salinity and Environmental Change in the Caspian-Black Sea-Mediterranean Corridor. The Geological Society of America Special Paper in press.

Palcu, D.V., Golovina, L.A., Vernyhorova, Y.V., Popov, S.V., Krijgsman, W., 2017. Middle Miocene paleoenvironmental crises in Central Eurasia caused by changes in marine gateway configuration. Glob. Planet. Chang 158, 57–71. https://doi.org/10.1016/j.gloplacha.2017.09.013.

Palmer, M.R., Edmond, J.M., 1989. The strontium isotope budget of the modern ocean. Earth Planet. Sci. Lett 92, 11–26.

Palo, J.U., Väinölä, R., 2006. The enigma of the landlocked Baikal and Caspian seals addressed through phylogeny of phocine mitochondrial sequences. Biol. J. Linn. Soc 88, 61–72.

Popov, S.V., Shcherba, I.G., Ilyina, L.B., Nevesskaya, L.A., Paramonova, N.P., Khondkarian, S.O., Magyar, I., 2006. Late Miocene to Pliocene palaeogeography of the Paratethys and its relation to the Mediterranean. Palaeogeogr. Palaeoclimatol. Palaeoecol 238, 91–106.

Ramstein, G., Fluteau, F., Besse, J., Joussaume, S., 1997. Effect of orogeny, plate motion and land-sea distribution on Eurasian climate change over the past 30 million years. Nature 386, 788–795.

Richards, K., Van Baak, C.G.C., Athersuch, J., Hoyle, T.M., Stoica, M., Austin, W.E.N., Cage, A.G., Wonders, A.A.H., Marret, F., Pinnington, C.A., 2018. Palynology and micropalaeontology of the Pliocene-Pleistocene transition in outcrop from the western Caspian Sea, Azerbaijan: potential links with the Mediterranean, Black Sea and the Arctic Ocean? Palaeogeogr. Palaeoclimatol. Palaeoecol 511, 119–143. https://doi.org/10.1016/j.palaeo.2018.07.018.

Rogerson, M., Rohling, E.J., Bigg, G.R., Ramirez, J., 2012. Paleoceanography of the Atlantic-Mediterranean exchange: overview and first quantitative assessment of climatic forcing. Rev. Geophys 50. https://doi.org/10.1029/2011RG000376.

Rohling, E.J., Foster, G.L., Grant, K.M., Marino, G., Roberts, A.P., Tamisiea, M.E., Williams, F., 2014. Sea-level and deep-sea-temperature variability over the past 5.3 million years. Nature 508, 477–482.

Rohling, E.J., Marino, G., Grant, K.M., 2015. Mediterranean climate and oceanography, and the periodic development of anoxic events (sapropels). Earth-Sci. Rev 143, 62–97. https://doi.org/10.1016/j.earscirev.2015.01.008.

Sant, K., Palcu, D.V., Mandic, O., Krijgsman, W., 2017. Changing seas in the Early–Middle Miocene of Central Europe: a Mediterranean approach to Parathyan stratigraphy. Terra Nova 29, 273–281. https://doi.org/10.1111/ter.12273.

Sejrup, H.-P., Guilbault, J.-P., 1980. Cassidulina reniforme and *C. obtusa* (Foraminifera), taxonomy, distribution, and ecology. Sarsia 65, 79–85. https://doi.org/10.1080/00364827.1980.10431476.

Sidnev, A.V., 1985. History of the development of the Pliocene hydrography in the Pred-Ural region. (in Russian).

Stoica, M., Lazar, I., Krijgsman, W., Vasiliev, I., Jipa, D.C., Floroiu, A., 2013. Palaeoenvironmental evolution of the East Carpathian foredeep during the late Miocene – early Pliocene (Dacian Basin; Romania). Glob. Planet. Chang 103, 135–148.

Sun, Y., Clemens, S.C., An, Z., Yu, Z., 2006. Astronomical timescale and palaeoclimatic implication of stacked 3.6-Myr monsoon records from the Chinese Loess Plateau. Quat. Sci. Rev 25, 33–48. https://doi.org/10.1016/j.quascirev.2005.07.005.

Van Baak, C.G.C., Vasiliev, I., Stoica, M., Kuiper, K.F., Forte, A.M., Aliyeva, E., Krijgsman, W., 2013. A magnetostratigraphic time frame for Plio-Pleistocene transgressions in the South Caspian Basin, Azerbaijan. Glob. Planet. Chang 103, 119–134.

Van Baak, C.G.C., Radionova, E.P., Golovina, L.A., Raffi, I., Kuiper, K.F., Vasiliev, I., Krijgsman, W., 2015. Messinian events in the Black Sea. Terra Nova 27, 433–441. https://doi.org/10.1111/ter.12177.

Van Baak, C.G.C., Stoica, M., Grothe, A., Aliyeva, E., Krijgsman, W., 2016. Mediterranean-Paratethys connectivity during the Messinian salinity crisis: the Pontian of Azerbaijan. Glob. Planet. Chang 141, 63–81. https://doi.org/10.1016/j.gloplacha.2016.04.005.

Van Baak, C.G.C., Krijgsman, W., Magyar, I., Sztanó, O., Golovina, L.A., Grothe, A., Hoyle, T.M., Mandic, O., Patina, I.S., Popov, S.V., Radionova, E.P., Stoica, M., Vasiliev, I., 2017. Paratethys response to the Messinian salinity crisis. Earth-Sci. Rev 172, 193–223. https://doi.org/10.1016/j.earscirev.2017.07.015.

Vasiliev, I., Reichart, G.-J., Davies, G.R., Krijgsman, W., Stoica, M., 2010. Strontium isotope ratios of the Eastern Paratethys during the Mio-Pliocene transition; Implications for interbasinal connectivity. Earth Planet. Sci. Lett 292, 123–131.

Vinogradov, A.P., 1969. Atlas of lithological-paleogeographical maps of the Soviet Union (in Russian). Vses. Aerogeol. Trest Mingeol. SSSR, Moscow.

Wang, X., Wei, H., Taheri, M., Khormali, F., Danukalova, G., Chen, F., 2016. Early Pleistocene climate in western arid central Asia inferred from loess-palaeosol sequences. Sci. Rep. 6, 1–9. https://doi.org/10.1038/srep20560.

Wegwerth, A., Dellwig, O., Kaiser, J., Ménot, G., Bard, E., Shumilovskikh, L., Schnetger, B., Kleinhanns, I.C., Wille, M., Arz, H.W., 2014. Meltwater events and the Mediterranean reconnection at the Saalian–Eemian transition in the Black Sea. Earth Planet. Sci. Lett 404, 124–135. https://doi.org/10.1016/j.epsl.2014.07.030.

Yanko, V., 1990. Stratigraphy and paleogeography of the marine Pleistocene and Holocene deposits of the southern seas of the USSR. Memorie della Società Geologica Italiana 44, 167–187.

Zhang, Z., Ramstein, G., Schuster, M., Li, C., Contoux, C., Yan, Q., 2014. Aridification of the Sahara desert caused by Tethys Sea shrinkage during the Late Miocene. Nature 513, 401–404. https://doi.org/10.1038/nature13705.